EPS-0494
Submitted to Pa 10,17 and Pl 1,2,3

Studies of the Hadronic Final State in Diffractive Deep–Inelastic Scattering Interactions at HERA

H1 Collaboration

Abstract

Measurements of the laboratory frame transverse energy (E_T) flow in deep–inelastic diffractive (DID) events are presented. These were made using the H1 detector at HERA. Comparisons are made between the E_T flow observed in diffractive and non-diffractive deep inelastic scattering (DIS) data, and with models assuming that DID results from electron–pomeron scattering, where the latter has partonic structure. No evidence is found for differences in the mechanism producing the E_T in DID and DIS events, once the effects of the differing electron–pomeron and electron–proton centre-of-mass energies have been allowed for. Evidence for hard partonic interactions in DID is seen in the transverse thrust distribution. DID jet production rates are measured and a significant level of two jet production observed. All data are well described by the above model of DID.

1 Introduction

The diffractive structure function of the proton, $F_2^{D(3)}$, has been measured for the first time at HERA [1, 2]. Analysis of this structure function demonstrates that diffractive deep inelastic scattering interactions (DID) are of a broadly scale invariant nature and thus presumably of partonic origin. Hence energy flows in such interactions are expected to be similar to those measured in non-diffractive deep inelastic scattering (DIS), once allowance has been made for the effects of any differences in the kinematic regimes studied, and they should be described to a similar level of accuracy by perturbative QCD and hadronization models. Here an investigation of the transverse energy flow in the laboratory frame for DID and DIS events is presented.

The data used were taken with the H1 detector at the HERA $e\,p$ collider at DESY in Hamburg, Germany. At HERA $E_p = 820$ GeV protons are brought into collision with $E_e = 26.7$ GeV electrons or positrons, giving a centre-of-mass energy of $\sqrt{s} = 296$ GeV . Direct comparisons of DID and DIS measurements are made and an investigation carried out into the degree to which the observed differences are due to the differing effective centre-of-mass energies of the DID and DIS systems. The expected E_T flow in a model in which DID is assumed to result from the interaction of the electron with a pomeron with partonic structure is also studied.

Further evidence for the partonic nature of DID is sought in the topology of the hadronic final state. The transverse thrust distribution, previously used to demonstrate the presence of hard underlying interactions in diffractive photoproduction [11], is examined for indications of the presence of interactions with a two body, "back-to-back" topology in DID. A search for the jets resulting from underlying parton interactions is made using a cone algorithm and requiring that the transverse energy of each jet in the hadronic centre of mass is $E_T^* > 5\,\mathrm{GeV}$. The rate of production of events with zero, one and two jets is determinied and compared with calculations in which DID is modelled as described above.

In the following, a coordinate system is used with origin at the interaction point and z axis along the proton beam, or forward direction. The pseudo–rapidity of a final state particle with polar angle θ is then $\eta = -\ln\tan\frac{\theta}{2}$.

2 Event selection

The selection of deep–inelastic scattering (DIS) events follows that used in our recent measurement of the proton structure function [3].

The event selection is based on the existence of a good electron candidate in the calorimeter with energy $E_{el} > 11\,\mathrm{GeV}$ and polar angle in the range $160 \leq \theta \leq 173^o$, and a reconstructed ep interaction point less than 30 cm away from the nominal position. The kinematical variables x_{Bj}, Q^2 and W^2 are reconstructed from the scattered electron. The sample is constrained to the kinematic region $W^2 > 3000\,\mathrm{GeV}^2$ in order to ensure a minimum amount of hadronic energy, and $Q^2 > 7.5\,\mathrm{GeV}^2$ such that the remaining contamination from beam–gas and photoproduction backgrounds are less than 2% of the total sample.

Two sub–samples are then identified from these DIS data. Diffractive DIS events, manifest at HERA as events in which there is an absence of energy flow in a region adjacent to the scattered proton or any proton remnant, are selected by demanding no activity above noise thresholds in detectors in the forward region of H1 [1]. Non–diffractive events are selected by requiring a minimum energy in the very forward region of the main calorimeter.

For diffractive DIS, two additional variables can be determined if the invariant mass of the hadronic final state (excluding the proton or any colourless remnant thereof), M_X, is measured in addition to the energy and angle of the scattered electron: $x_{I\!P}$, the momentum fraction of the proton carried by the diffractive exchange, and β, the Bjorken–x variable for deep–inelastic scattering off the diffractive exchange [1].

Simulations of DIS events are used to correct the data for the inefficiency and finite resolution of the detector such that the measurements presented represent estimates of the energy flow distributions before interaction with the detector.

Non–diffractive DIS was simulated using the LEPTO program [7], which uses the colour dipole model (CDM) as implemented in ARIADNE [8]. The simulated Monte Carlo events were subjected to the same reconstruction and analysis chain as the real data.

Diffractive DIS was simulated using the RAPGAP program [9]. The pomeron structure was taken to be due to both a hard ($\propto z(1-z)$ where $z = x_{i/I\!P}$, the momentum fraction of the pomeron carried by the parton i) quark distribution and a hard gluon distribution, with quark ($i = q$) and gluon ($i = g$) induced processes contributing equally to the cross section. Such an admixture is consistent with the measurement of $F_2^{D(3)}$.

The study of transverse energy flow is based upon data taken during 1993, amounting to an integrated luminosity of $271 \pm 14\,\mathrm{nb}^{-1}$. The analysis of jets and transverse thrust takes advantage of the larger data sample amassed during 1994, corresponding to $\sim 2\,\mathrm{pb}^{-1}$.

3 Inclusive transverse energy flow

Within the framework of the naïve Quark-Parton-Model (QPM), the measurement of the momentum of the scattered electron determines the expected direction of the struck quark. In the laboratory system the corresponding pseudo-rapidity η_q can be written as

$$\eta_q = \frac{1}{2}\ln\left[x_{Bj}\left(\frac{x_{Bj}s}{Q^2} - 1\right)\frac{E_p}{E_e}\right]. \qquad (1)$$

In the following, the measured transverse energy flow in the laboratory frame is studied with respect to this direction. The errors included for the energy flow data include both statistical and systematic uncertainties. The most significant sources of systematic error are:

- uncertainty in the measurement of the electron energy and angle
- uncertainty in the energy scale for the measurement of hadrons in the calorimeters

- the dependence of the corrections applied to the data on the adoption of hadronisation schemes other than the colour dipole model in the Monte Carlo calculations
- the influence of QED radiative effects on the reconstruction of the event kinematics.

At large values of x_{Bj} the largest uncertainty results from the accuracy with which we know the electron energy, while at small values of x_{Bj} no single source of error dominates.

In figures 1a) and 1b) the transverse energy flows are plotted for $x_{Bj} < 10^{-3}$ and $x_{Bj} > 10^{-3}$ respectively, where η is the pseudo–rapidity of the energy deposit in the calorimeter. For both diffractive and non–diffractive data, there is a visible shift of the central peak position away from the naïve QPM prediction (equation 1). This shift is characteristic of the probing of coloured structure within a colourless object (be it a proton in the non–diffractive case, or a colourless component of the proton in the diffractive case). A colour field then exists between the struck component of the colourless object and the coloured remnant leading to the production of hadronic energy in the region between the struck component and the remnant.

Comparing diffractive with non-diffractive events, it is observed that the current region (around $\Delta\eta \approx 0$) is similar for both sets of events. The maxima in transverse energy flow are of similar magnitudes. The observed shift from the naïvely expected position of the maximum is positive in both cases, and is smaller for diffractive events than non–diffractive events. In the case of diffractive DIS events the level of transverse energy in the forward region is significantly lower than for non–diffractive events.

Also shown are the MC models used for to correct for detector effects. In both cases, the data are described reasonably well, although deviations are visible in the region of the current peak for non-diffractive DIS.

4 Parametrization of transverse energy flow

To investigate of the dependence of the transverse energy flow on the event kinematics, estimators of the basic properties of the measured hadronic final state are determined for each event.

Four parameters have been chosen. They are calculated for each event from the transverse energy flow as measured in the calorimeters as follows:

$$\Delta\eta_{ev} = \frac{\sum\limits_{|\Delta\eta|<2,|\Delta\phi|<1.5} E_T \Delta\eta}{\sum\limits_{|\Delta\eta|<2,|\Delta\phi|<1.5} E_T} \tag{2}$$

$$E_{Tpeak} = \frac{1}{0.5} \sum_{|\eta-(\eta_q+\Delta\eta_{ev})|<0.25} E_T \tag{3}$$

$$\sigma^2_{peak} = \frac{\sum\limits_{|\eta-(\eta_q+\Delta\eta_{ev})|<1} E_T [\eta - (\eta_q + \Delta\eta_{ev})]^2}{\sum\limits_{|\eta-(\eta_q+\Delta\eta_{ev})|<1} E_T} \tag{4}$$

$$E_{T forw} = \frac{1}{3 - (\eta_q + \Delta\eta_{ev} + 1)} \sum_{(\eta_q + \Delta\eta_{ev} + 1) < \eta < 3} E_T. \qquad (5)$$

The summations are performed over all calorimeter cells within the specified ranges.

$\Delta\eta_{ev}$ quantifies the shift in pseudo-rapidity of the observed maximum of the transverse energy distribution from the naïvely expected direction, η_q. $E_{T peak}$ gives the magnitude of the energy flow in the region of the current jet, that is, around the position $\Delta\eta = \Delta\eta_{ev}$. The width of the current peak is represented by using σ_{peak}. A measure of the level of transverse energy away from the current region towards the proton remnant direction is given by $E_{T forw}$.

Figure 3 shows the dependence of the four estimators on the kinematical variable x_{Bj}, for non–diffractive and diffractive DIS events. Similarities in the energy flows of the two sets of DIS events are clearly visible. The magnitude and width of the current peak show the same dependences on x_{Bj} in both cases. It is possible that any small differences between the magnitude of the peak shift and the level of energy flow in the forward region between the diffractive and non–diffractive data may be attibutable to the differing centre of mass energies of the electron–proton and the electron–pomeron systems.

This hypothesis may be tested by comparing the diffractive data with the the standard deep–inelastic Monte Carlo (LEPTO+ARIADNE) simulation with a reduced proton beam energy of 2.46 GeV (varying this between 0.82 and 8.2 GeV) such that the invariant mass W of the photon-proton system is comparable to the invariant mass M_X of the hadronic final state attributed to the photon–pomeron system. Thus the proton plays the rôle of a pomeron in the kinematic range $10^{-3} < x_{I\!P} < 10^{-2}$. Figure 4 shows the dependence for the diffractive data of $\Delta\eta_{ev}$ and $E_{T forw}$ on the variable β, which is the relevant Bjorken–x variable for the photon–pomeron system. A peak shift of up to 0.8 units of (laboratory) pseudo–rapidity is observed for the diffractive data. The data are well reproduced by the "mini–HERA" calculation.

Thus there is no evidence that the QCD dynamics responsible for producing the energy flow in the diffractive and non–diffractive events differ in any way. In particular, we find no evidence for any anomaly in the level of QCD radiation.

5 Hard interactions in diffractive DIS

Transverse thrust may be used to study the topology of the hadronic final state in diffractive processes. Transverse thrust $T_\perp = \max\left(\sum \mathbf{P_T} \cdot \mathbf{n} / \sum |\mathbf{P_T}|\right)$, calculated using charged tracks and calorimeter clusters in the $\gamma^* I\!P$ centre of mass system, is a measure of the extent to which a system is "back–to–back". At low transverse masses there are few particles produced and fluctuations may result in high values of $T_\perp$. For processes in which there is no underlying structure (no hard interaction), $T_\perp$ will fall with increasing transverse mass to an asymptotic limit of $2/\pi$.

The mean transverse thrust is shown as a function of transverse mass, M_T, for deep–inelastic diffractive scattering events in figure 5. This distribution has not been corrected for detector effects. M_T is the total invariant mass of the projections of the event momentum vectors onto the plane transverse to the proton axis in the $\gamma^* I\!P$ centre of mass

system. The expected fall with increasing M_T is observed at low M_T. At $M_T \sim 8\,\mathrm{GeV}$, the transverse thrust begins to rise again. This is unambiguous evidence for a two body, back–to–back structure (such as a hard interaction) that begins to be observable for transverse masses of $\sim 8\,\mathrm{GeV}$ and above.

Given that there is evidence for hard interactions, an attempt may be made to reconstruct the momenta of the outgoing partons from the hard scattering process by identifying the jets resulting from these partons.

This study was performed in the $\gamma^* I\!P$ centre of mass system, denoted by the superfix *. A cone jet algorithm [10] was used. The investigated range in pseudorapidity η^* was $-2.5 \leq \eta^* \leq 2.5$. The grid in the η^*–ϕ^* plane was divided into 25×24 cells and a minimal E_t^* of 5 GeV for a jet candidate was required. A cone radius $R^* = \sqrt{(\Delta\eta^*)^2 + (\Delta\phi^*)^2}$ of $R^* = 1$ was used.

Approximately 100 events with two or more jets were found in the data. Figure 7 shows the jet profiles in $\Delta\eta^* = \eta^*_{\mathrm{particle}} - \eta^*_{\mathrm{jet}}$ and $\Delta\phi^* = \phi^*_{\mathrm{particle}} - \phi^*_{\mathrm{jet}}$ for the two jet events. The bulk of the transverse energy flow is close to the jet axes, in agreement with a QCD calculation made using RAPGAP with a pomeron whose structure is predominantly gluonic. Figure 6 shows the correlation ϕ^*, η^*, and E_T^* between the reconstructed jets and the partons emerging from the hard subprocess, using this same calculation. It is evident that the kinematics of the underlying hard interactions are reconstructed meaningfully by the jet finding procedure used.

The relative rates for zero, 1 and 2 jet production, uncorrected for acceptance effects and experimental bias, are shown as a function of the total mass of the hadronic system. As M_X rises and the phase space for multi–jet production rises, the relative rate of 2 jet events rises, to $\sim 15\%$ at $M_X = 35\,\mathrm{GeV}$. The data are well described by the RAPGAP Monte Carlo simulations in which both quarks and gluons enter the hard scattering process. It is, however, premature to draw detailed conclusions about the partonic content of the pomeron without a detailed study of the effects of evolution and higher order processes.

The method of selecting diffractive events using detectors in the forward region of H1 permits the study of multi–jet production for values of M_X up to 40 GeV or more. Figure 9 shows the distribution of η_{max}, the (laboratory) pseudo–rapidity of the most forward energy cluster with energy greater than 0.4 GeV. The level of background from non–diffractive processes is small for all except the very highest masses, typically corresponding to the largest values of laboratory frame η_{max}, where the background never exceeds 20%.

6 Conclusions

A detailed investigation of the energy flow associated with the hadronic final state of DIS events shows striking similarities between diffractive and non-diffractive events. If the diffractive events are ascribed to the interaction of a virtual photon with a pomeron composed of partonic constituents, then there is no evidence for any significant difference in the underlying dynamics in the subsequent generation of the hadronic final state in diffractive deep-inelastic scattering compared to non–diffractive deep–inelastic scattering. In particular we see no evidence for any suppression of gluon radiation in the diffractive

sample with respect to that expected for standard deep–inelastic scattering processes at the same energy scale. The is confirmed by the observation that the measured data are reproduced well by a model ascribing diffractive DIS to the interaction of electrons with a pomeron with partonic structure.

An analysis of transverse thrust provides evidence for the presence of hard scattering processes in deep–inelastic diffractive scattering.

Using a CONE jet algorithm with a minimum E_T^* requirement of 5 GeV for each jet, approximately 100 events with 2 jets are observed in the data for total hadronic masses of up to ~ 40 GeV. These jets are well described by Monte Carlo simulations based on hard interactions between the virtual photon and partonic constituents of the pomeron.

Acknowledgements

We are grateful to the HERA machine group whose outstanding efforts made this experiment possible. We appreciate the immense effort of the engineers and technicians who constructed and maintained the detector. We thank the funding agencies for their financial support of the experiment. We wish to thank the DESY directorate for the support and hospitality extended to the non-DESY members of the collaboration.

References

[1] H1 Collab., T. Ahmed et al., Phys. Lett. **B348** (1995) 681.

[2] ZEUS Collab., M. Derrick et. al., DESY preprint 95-093.

[3] H1 Collab., T. Ahmed et al., Nucl. Phys. **B439** (1995) 471.

[4] ZEUS Collab., M. Derrick et al., Phys. Lett. **B315** (1993) 481.

[5] H1 Collab., T. Ahmed et al., Nucl. Phys. **B429** (1994) 477.

[6] H1 Collab., I. Abt et al., DESY preprint 93-103 (1993), to be published in Nucl. Instr. and Meth.

[7] G. Ingelmanm Proceedings of the Workhop Physics at HERA, vol. 3, eds. W. Buchmüller, G. Ingelman, DESY (1992) p. 1366.

[8] L. Lönnblad, Comp. Phys. Comm. **71** (1992) 15.

[9] H. Jung, Comp. Phys. Comm. **86** (1995) 147.

[10] CDF Collab., F. Abe et al., Phys. Rev. **D45** (1992) 1448.

[11] H1 Collab., T. Ahmed et. al., Nucl. Phys. **B435** (1995) 3.

[12] ZEUS Collab., M. Derrick et. al., Phys. Lett. **B346** (1995) 399.

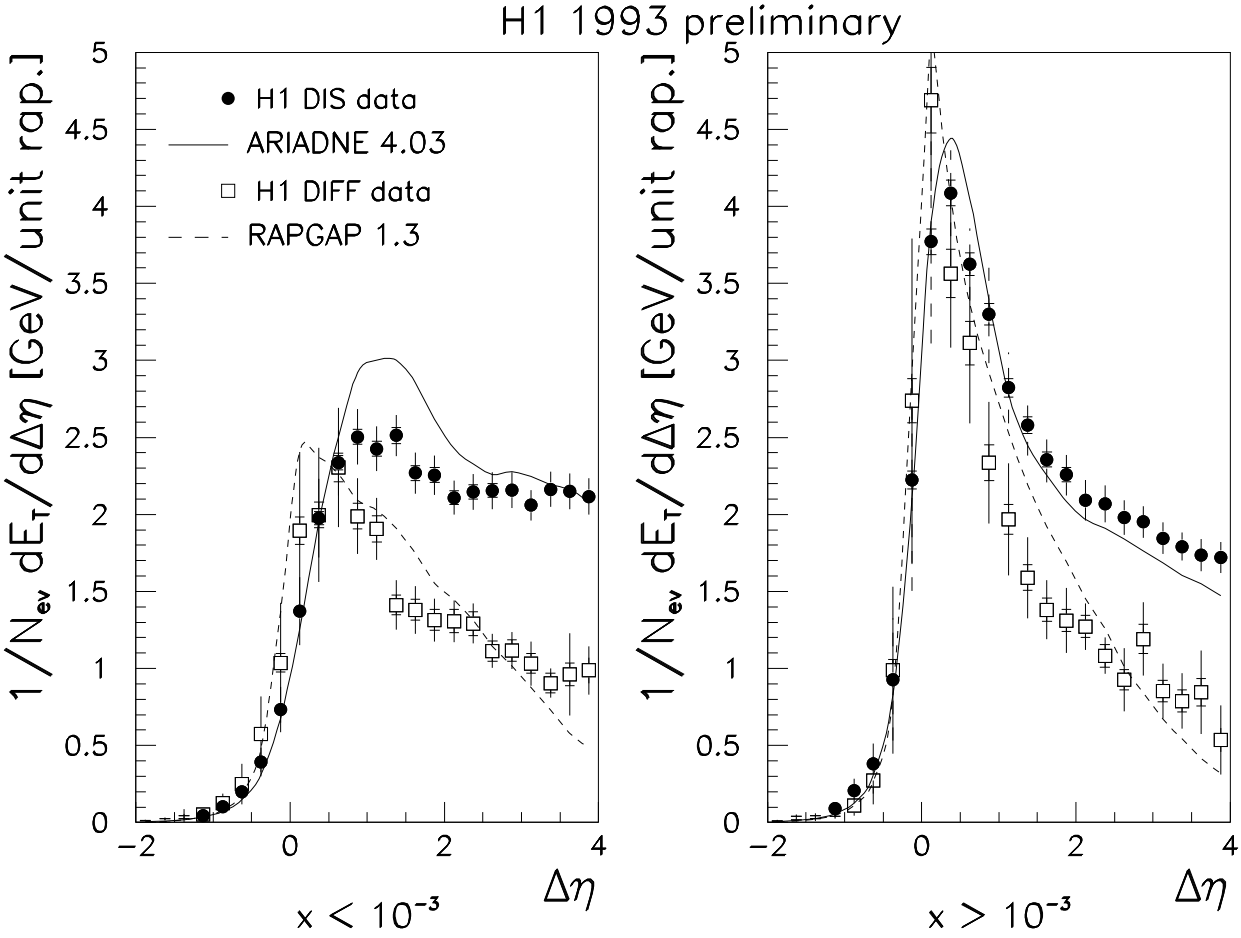

Figure 1: Measured Transverse Energy Flow (corrected for detector effects) around the expected directions from the naive QPM. Shown are non-diffractive events as well as diffractive events, both having been corrected for detector effects. Also indicated are a Monte Carlo model for DIS (CDM) and a Monte Carlo model for diffractive DIS (RAPGAP). The left figure shows events with $x_{Bj} < 10^{-3}$, whereas the right one includes only events with $x_{Bj} > 10^{-3}$. In both plots the proton direction corresponds to $\Delta\eta > 0$. The inner error bar is the statistical error; the full error shows the statistical and systematic error added in quadrature.

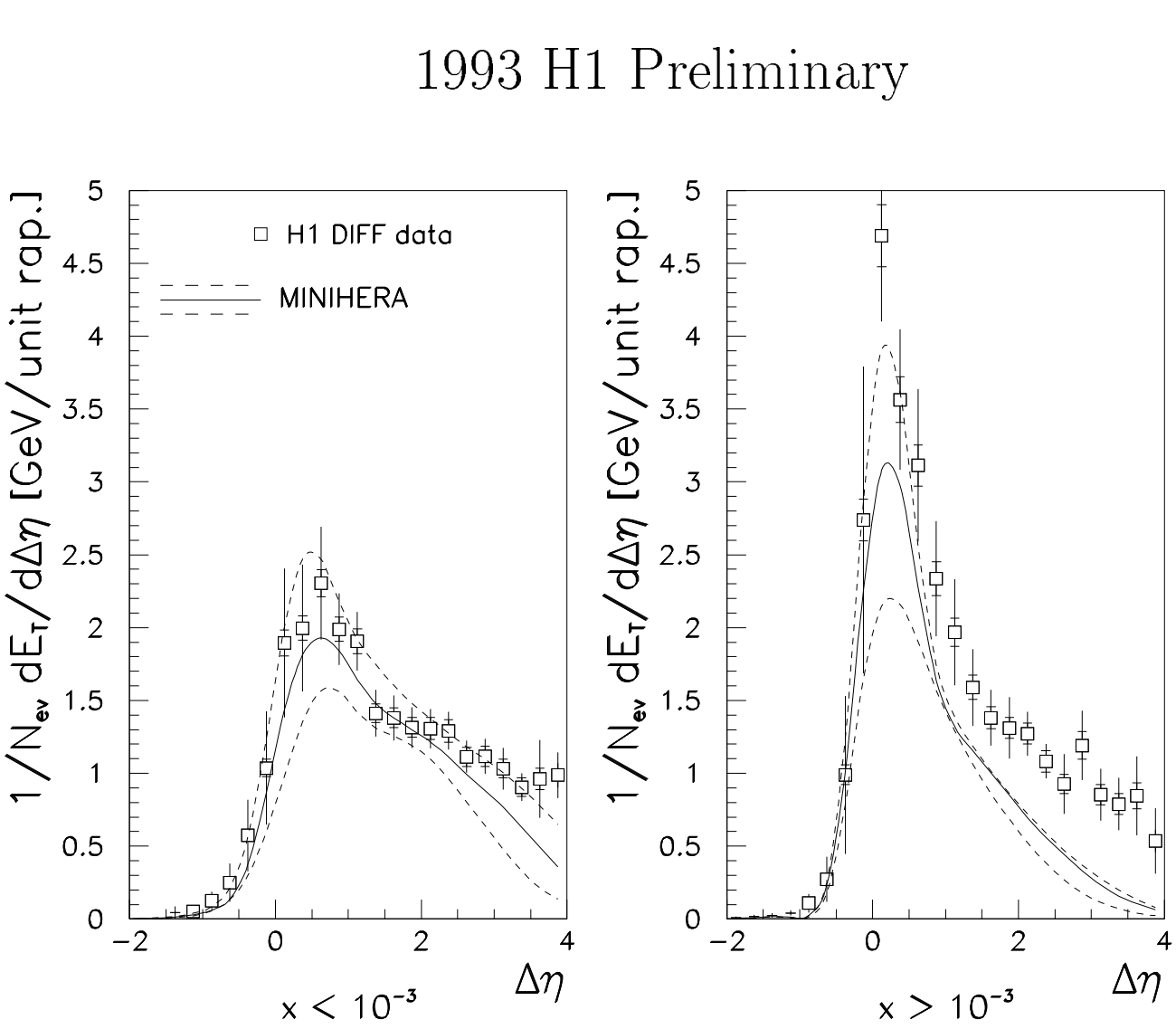

Figure 2: Measured Transverse Energy Flow (corrected for detector effects) around the expected directions from the naive QPM. Shown are the diffractive events, corrected for detector effects. Also show is the prediction from the "mini–HERA" model, in which the standard DIS Monte Carlo (CDM) was run with the proton beam energy set to 2.46 GeV (solid line), 0.82 GeV and 8.2 GeV (dashed lines). The left figure shows events with $x_{Bj} < 10^{-3}$, whereas the right one includes only events with $x_{Bj} > 10^{-3}$. The mean Q^2 values are is 12.7 GeV^2 for the low–x bin and 28.2 GeV^2 for the high–x bin. In both plots the proton direction corresponds to $\Delta\eta > 0$. The inner error bar is the statistical error; the full error shows the statistical and systematic error added in quadrature.

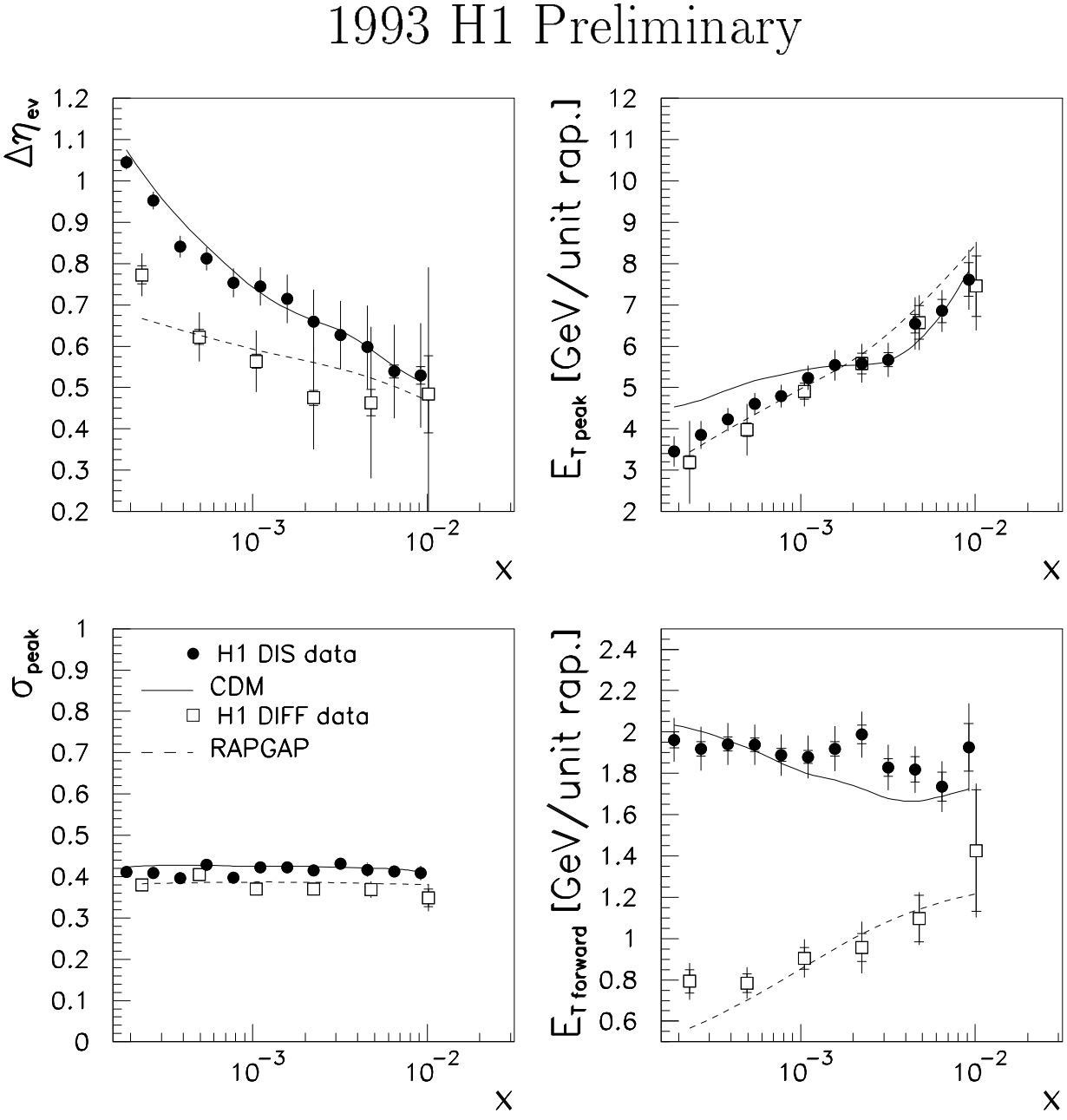

Figure 3: Measured estimators of transverse energy flow for non-diffractive (closed circles) and diffractive DIS events (open circles), compared with the CDM (solid line) and RAPGAP (dashed line) Monte Carlo models (see text). The parameters are plotted as a function of x_{Bj}. The inner error bar is the statistical error; the full error shows the statistical and systematic error added in quadrature.

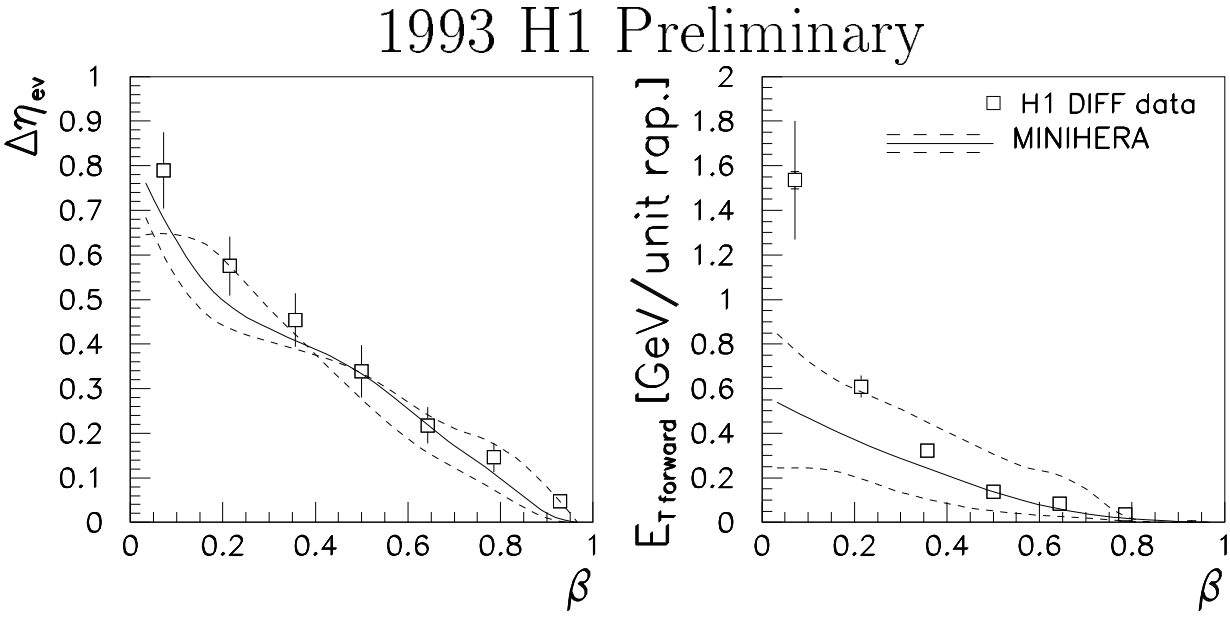

Figure 4: Measured parameters for diffractive DIS events, compared to a model calculation of e-p collisions with a reduced proton beam energy ("mini–HERA") plotted as a function of the relevant Bjorken–x variable. The solid line represents the calculation with a proton beam energy of 2.46 GeV, the upper and lower dashed lines represent proton beam energies of 8.2 GeV and 0.82 GeV respectively. The inner error bar is the statistical error; the full error shows the statistical and systematic error added in quadrature.

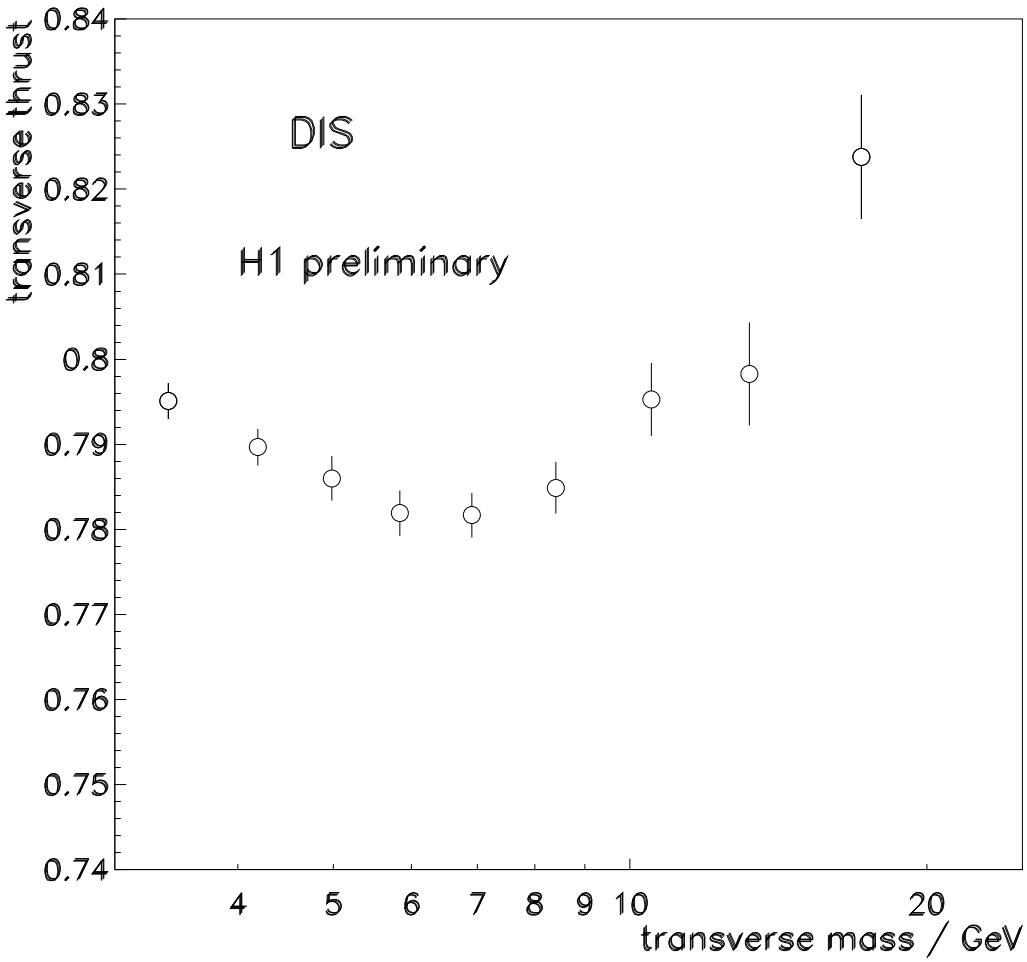

Figure 5: Dependence of the transverse thrust of the transverse mass in diffractive DIS events. The data are not corrected for the effects of finite acceptance or resolution. Only statistical errors are shown.

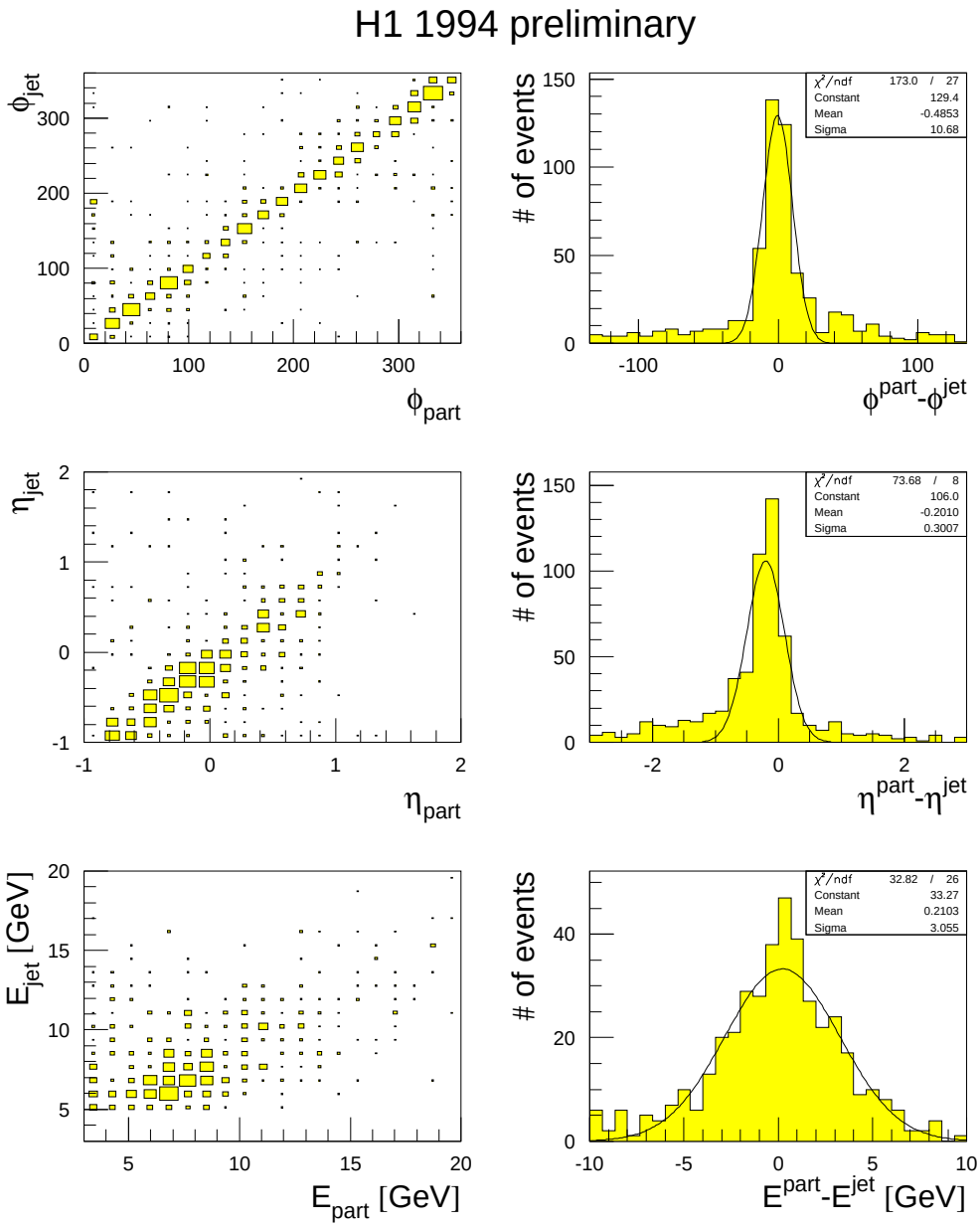

Figure 6: Correlation between jet and parton kinematics for the CONE algorithm applied to the RAPGAP gluon Monte Carlo ($\gamma^*\mathbb{P}$ cm). For the observables ϕ, η and E the correlation is shown as box plots (left column) and as resolution plots (right column).

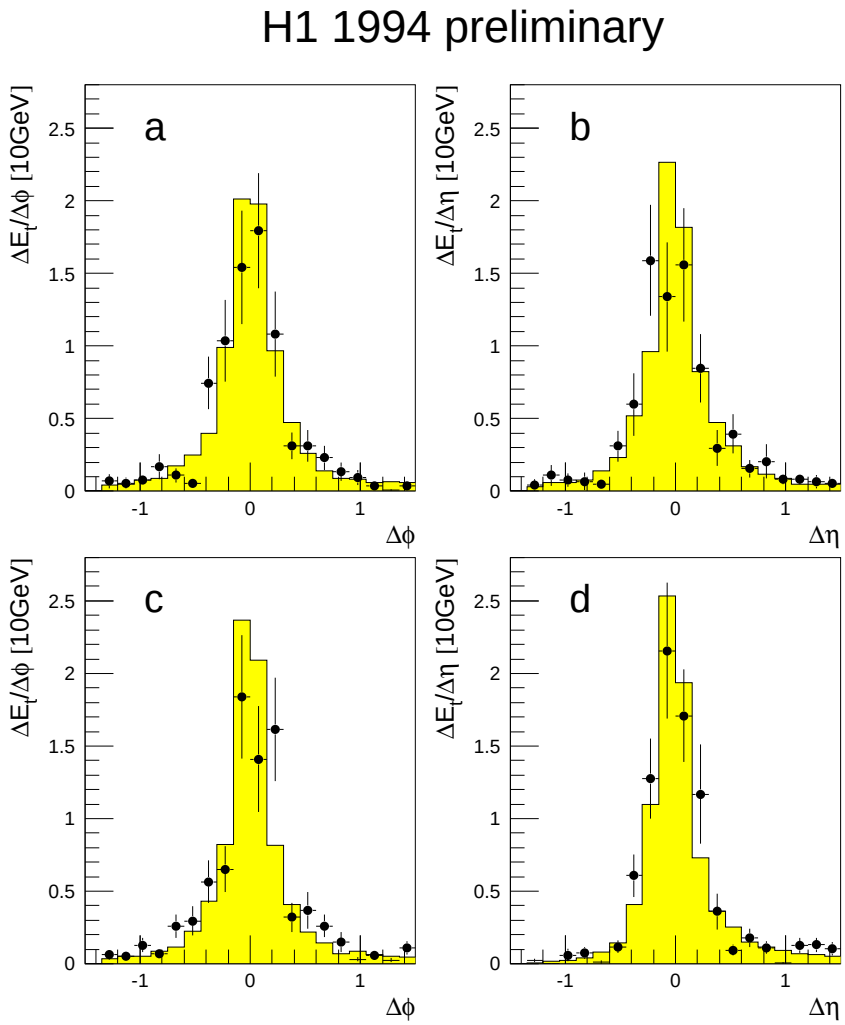

Figure 7: Jet profiles in the γ^*IP cms for H1 diffractive data (circles) and RAPGAP gluon (histograms) using the CONE algorithm: profiles in $\Delta\phi$ (a,c) and $\Delta\eta$ (b,d) for the more forward (a,b) and the more backward (c,d) jet of events with exactly two jets in this frame. Only statistical errors are shown.

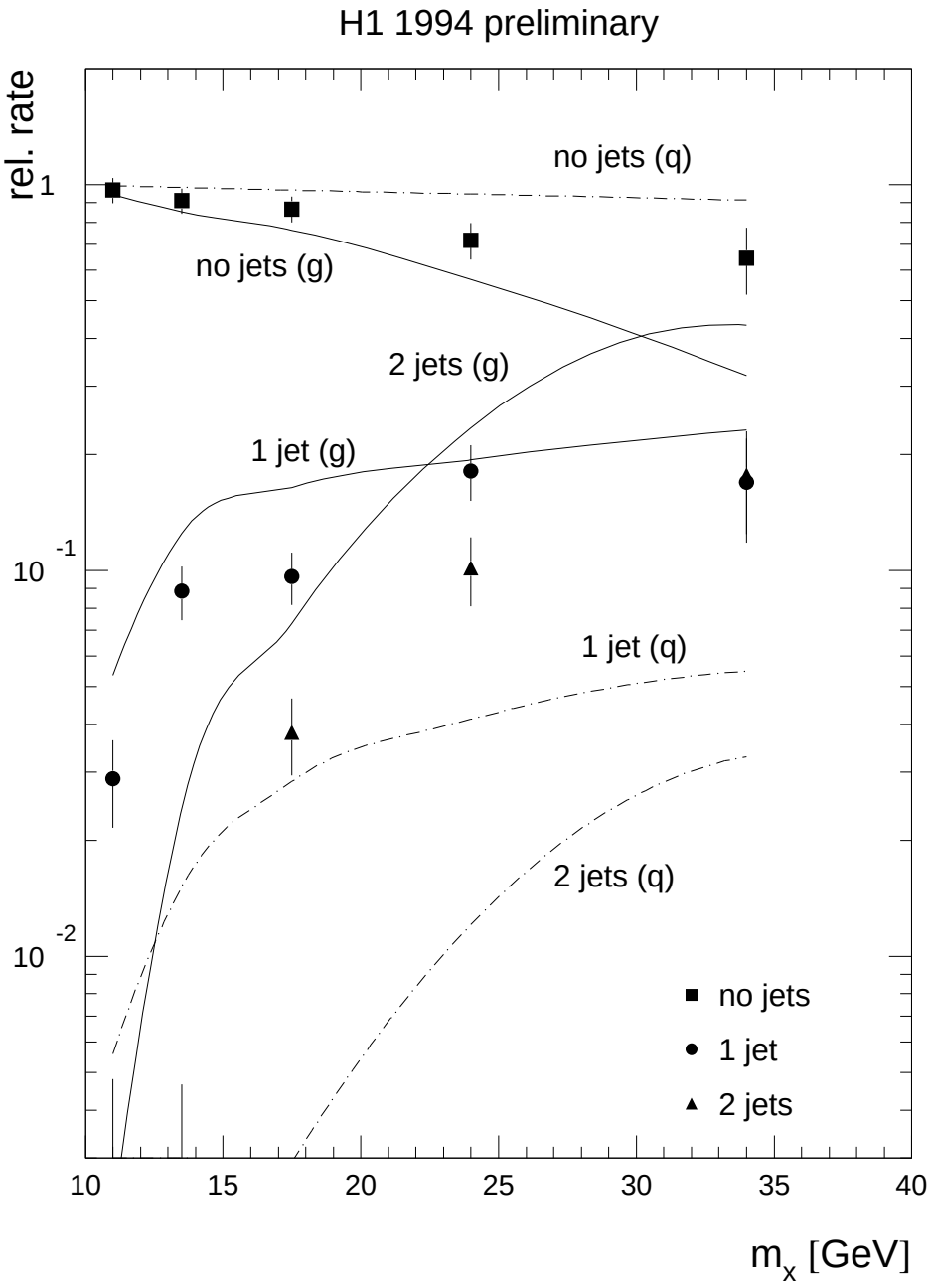

Figure 8: Relative jetrates in the $\gamma^*\mathbb{P}$ cms as function of the invariant mass of the hadronic final state, M_x, for the RAPGAP gluon monte carlo (solid lines), the RAPGAP quark monte carlo (dashed lines) and the diffractive data (symbols with error bars). Symbols are events with no jets (squares), one jet (circles) and two jets (triangles). Only statistical errors are shown.

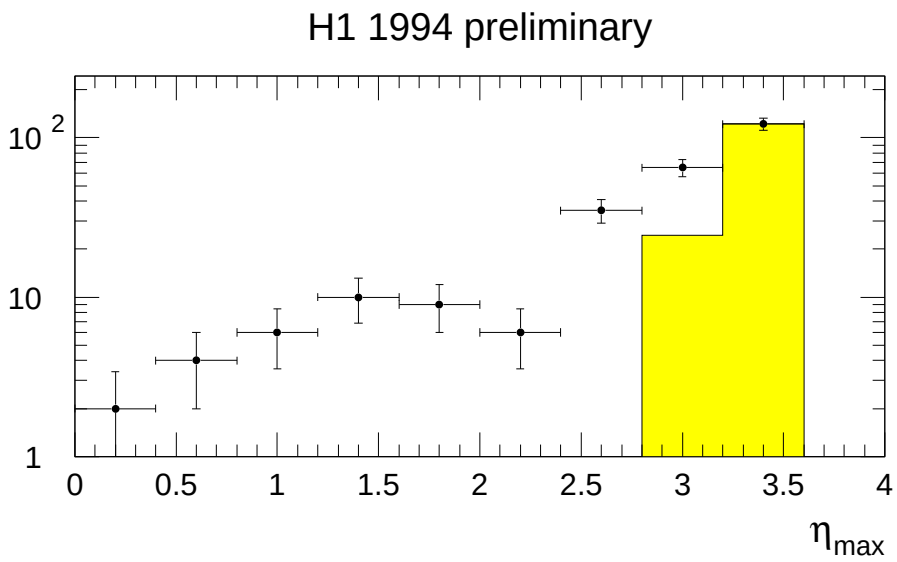

Figure 9: The distribution of η_{max}, the pseudo–rapidity of the energy deposition in the main calorimeter above 400 MeV closest to the proton beam direction. The points are the data with two jets, each with transverse energy above 5 GeV. The shaded histogram represents the contribution from non–diffractive processes, estimated with Monte Carlo. A cut is made at $\eta_{max} < 3$ to select diffractive events. Only statistical errors are shown.